Inorganic Gyroid with Exceptionally Low Refractive Index from Block Copolymer Templating

ARTICLE *in* NANO LETTERS · NOVEMBER 2010

Impact Factor: 13.59 · DOI: 10.1021/nl103104w · Source: PubMed

8 AUTHORS, INCLUDING:

Han-Yu Hsueh
University of Massachusetts Amherst
15 PUBLICATIONS **232** CITATIONS
SEE PROFILE

Shangjr Gwo
National Tsing Hua University
123 PUBLICATIONS **2,161** CITATIONS
SEE PROFILE

Hirokazu Hasegawa
Kyoto University
163 PUBLICATIONS **4,951** CITATIONS
SEE PROFILE

Edwin L Thomas
Rice University
621 PUBLICATIONS **24,504** CITATIONS
SEE PROFILE

NANO LETTERS

pubs.acs.org/NanoLett

Inorganic Gyroid with Exceptionally Low Refractive Index from Block Copolymer Templating

Han-Yu Hsueh,[†] Hung-Ying Chen,[‡] Ming-Shiuan She,[†] Chun-Ku Chen,[†] Rong-Ming Ho,*[,†] Shangjr Gwo,[‡] Hirokazu Hasegawa,[§] and Edwin L. Thomas[||]

[†] Department of Chemical Engineering and [‡] Department of Physics, National Tsing Hua University, Hsinchu 30013, Taiwan, [§] Department of Polymer Chemistry, Graduate School of Engineering, Kyoto University, Nishikyo-ku, Kyoto, 615-8510, Japan, and [||] Department of Materials Science and Engineering, Massachusetts Institute of Technology, Cambridge, Massachusetts 02139, United States

ABSTRACT Nanoporous polymers with gyroid nanochannels can be fabricated from the self-assembly of degradable block copolymer, polystyrene-*b*-poly(L-lactide) (PS-PLLA), followed by the hydrolysis of PLLA blocks. A well-defined nanohybrid material with SiO_2 gyroid nanostructure in a PS matrix can be obtained using the nanoporous PS as a template for sol-gel reaction. After subsequent UV degradation of the PS matrix, a highly porous inorganic gyroid network remains, yielding a single-component material with an exceptionally low refractive index (as low as 1.1).

KEYWORDS Sol-gel process, low-n materials, degradable block copolymers, templates, gyroid

Porous materials whose properties depend on their individual components and morphologies are potentially next generation materials because of their excellent material characteristics, including optical, electrical, optoelectronic, and mechanical properties. Some porous materials, such as nuclear track-etched polycarbonate membrane[1] and anodized aluminum oxide films,[2] have been used in various fields. However, their micrometer-size cylinder shapes are limited for applications in nanotechnologies. Precise control of the geometries of the pores with nanometer-size dimension in such porous materials is critical to optimizing their performance, but this goal remains difficult to achieve.

In recent decades, block copolymers (BCPs) have been extensively investigated because of their ability to self-assemble into one-, two-, or three-dimensional periodic nanostructures, according to their constituted compositions. BCPs that consist of chemically different components can self-assemble into various ordered nanostructures such as sphere, cylinder, gyroid, and lamellae, owing to the incompatibility of constituted blocks with a readily adjustable size scale dependent on molecular weight.[3,4] Consequently, well-defined nanostructures can be tailored by the molecular engineering of synthetic BCPs with promising features for applications in nanotechnologies. By taking advantage of the degradable character of constituted components, nanoporous polymers could be fabricated from self-assembled BCP nanostructures by the selective degeneration of one of the constituted blocks.[5−10] As a result, chemically degradable BCPs that can form nanoporous polymers have drawn considerable attention for use in nanofabrication. Polylactide-containing BCPs (such as polystyrene-*b*-poly(D,L-lactide) (PS-PLA) and polystyrene-*b*-poly(L-lactide) (PS-PLLA)) are highly suited to the fabrication of nanoporous polymers because of the unstable character of the ester group, which can be hydrolytically decomposed.[8,11]

Among all of the nanostructures formed by the self-assembly of BCPs, the gyroid is one of the most appealing morphologies for practical applications because of its unique geometry, comprising a matrix and two continuous but independent, interpenetrating networks in three-dimensional space; as a result, it is also referred to a double gyroid nanostructure.[12−14] After the selective degeneration of the minority block, the gyroid nanostructure could be exploited to create fully interconnected nanochannels. Because of high porosity and specific surface, the nanoporous polymes resulting from the BCP gyroid are very promising for use in a variety of applications, such as photonic crystals,[15,16] catalysts,[9] ceramic membranes,[10,17,18] membrane reactors,[19−22] and hybrid solar cells.[23]

Nanoporous materials with a nanostructured surface topology can be applied as optical and electronic materials because of their transparent character with a feature scale smaller than the wavelength of the incoming light, and also low refractive index and dielectric constant. The refractive indices of porous materials are related to the degree of porosity and to the refractive indices of the corresponding nonporous, dense materials. Because of their low refractive

* To whom correspondence should be addressed. Tel: 886-3-5738349. Fax: 886-3-5715408. E-mail: rmho@mx.nthu.edu.tw.

Received for review: 09/2/2010
Published on Web: 11/03/2010

DOI: 10.1021/nl103104w | *Nano Lett.* **2010,** *10,* 4994–5000

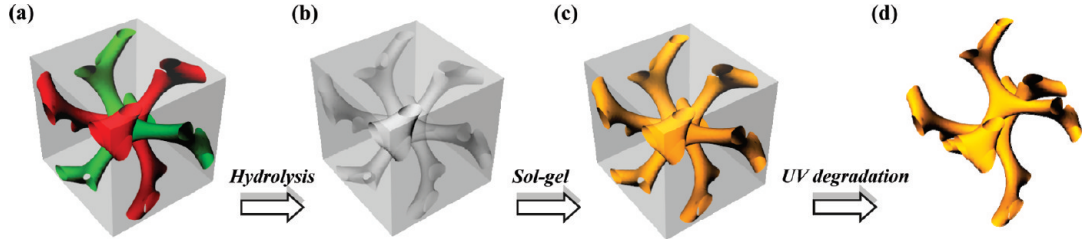

FIGURE 1. Schematic illustration for the creation of well-defined nanoporous gyroid SiO_2 from BCP templating. (a) PS-PLLA gyroid morphology (skeleton of double gyroid structure with two identical networks (green and red)). (b) Gyroid-forming nanoporous PS template after the removal of minority PLLA network. (c) PS/SiO_2 gyroid nanohybrids via the templated sol−gel process. (d) Nanoporous gyroid SiO_2 after the UV removal of PS template.

index (low-n) properties, nanoporous materials have been extensively exploited for optical applications such as antireflection properties. Antireflection structures (ARS) are used to restrict the reflection of light from the surface of optical components and to improve transmission. For example, in the near-infrared region, the reflection loss of a silicon solar cell in air is ~30% at normal incidence. Thus, achieving a way to reduce the reflection loss would be of interest for Si-based solar cell and optoelectronic device applications. The ARS is essential to optical applications, such as solar cells,[24] omnidirectional reflectors,[25] air-ambient,[26] optical components,[27] light-emitting diodes,[28] and other optoelectronic devices.

The simplest ARS should be designed with a single-layer material for destructive interference. To eliminate the reflection at the interface between air and the ARS, two requirements should be satisfied. First, $n_a \leq (n_s n_i)^{1/2}$ in which n_a, n_s, and n_i are the refractive indices of the ARS, substrate, and air, respectively. Second, the ARS thickness must be one-quarter of the incidence wavelength in the optical medium. The refractive index of a typical substrate such as glass is approximately 1.5. So, the refractive index of the ARS must be smaller than 1.22. However, the refractive indices of dense solid materials are too large to match the refractive index of air. The lowest refractive indices of dense materials (MgF_2) are about the order of 1.35. A single ARS cannot have a refractive index of this value.

Accordingly, porous materials are used in broadband ARS, by taking advantage of the low refractive index of air ($n \sim 1$) voids. Hybrid configurations, like those of porous sol−gel[29,30] and optical polymeric thin-film coatings with small pores, have been developed.[31−33] For instance, Steiner et al. demonstrated excellent control of film thicknesses under a few hundred nanometers, as well as the control of pore sizes, by blending PS and poly(methyl methacrylate) (PMMA) for spinodal decomposition by phase separation followed by the selective removal of the PS blocks.[31] Furthermore, Kim et al. demonstrated that the pore volume of ARS made from degradable BCPs could be easily controlled because of the well-defined volume fraction of the degradable block in a BCP and the development of nanostructures from microphase separation.[32] Cho et al. also demonstrated ARS by using nanoporous films resulting from the layer-by-layer assembly of two BCP micelles on substrates.[33] However, the ARS made from polymers suffers from strong absorbance and radiation damage. Other approaches for fabricating an ARS have also been demonstrated, such as electron-beam writing,[34] alignment of liquid crystals,[35,36] and interference lithography.[37] Subwavelength period gratings called "moth-eye structures" have been designed and fabricated as optical devices based on both theoretical and experimental studies.[38−40]

In this study, we demonstrate that an inorganic nanoporous material with high porosity and well-defined periodic nanostructure can be fabricated from the self-assembly of a PS-PLLA BCP followed by the hydrolysis of PLLA blocks, templating silica networks via the sol−gel process and finally UV removal of the PS. Figure 1 shows this method. A PS-PLLA BCP with a molecular weight of 61 000 g mol^{-1} and a PLLA volume fraction of 39% was synthesized (see Supporting Information for details). The microdomain structure consists of the two three-dimensional (3D) continuous PLLA networks. Since the PLLA blocks are in a continuous structure, they can be easily degenerated by hydrolysis. After hydrolytic treatment, nanoporous PS matrix can be formed and used as a template for the sol−gel reaction. Useful ceramic oxides including the oxides of Al, Si, Ti, Zn, and Zr can be synthesized through the sol−gel process.[41] Although MgF_2 and CaF_2 are the materials with lower refractive indices and can be formed by the sol−gel process, they are slightly toxic. As a result, SiO_2 resulting from the sol−gel process is a better candidate as the inorganic low-n materials from the BCP template. Notably, dense amorphous SiO_2 with an index of 1.45 is one of the naturally occurring materials with a low refractive index and low absorbance. Furthermore, the amorphous SiO_2 formed by the sol−gel process has a lower refractive index than that of dense SiO_2 because of the existence of voids in the SiO_2 matrix after solvent evaporation.[30] Consequently, the formation of a single-component inorganic material with an exceptionally low refractive index (as low as 1.1) can be achieved.

Results and Discussion. Bulk samples of the PS-PLLA gyroid were prepared by solution casting. After quenching from microphase-separated ordered melt, the thermally treated BCPs were sectioned by an ultramicrotome for TEM observation. Figure 2a shows the projection image of the

DOI: 10.1021/nl103104w | *Nano Lett.* **2010,** *10,* 4994–5000

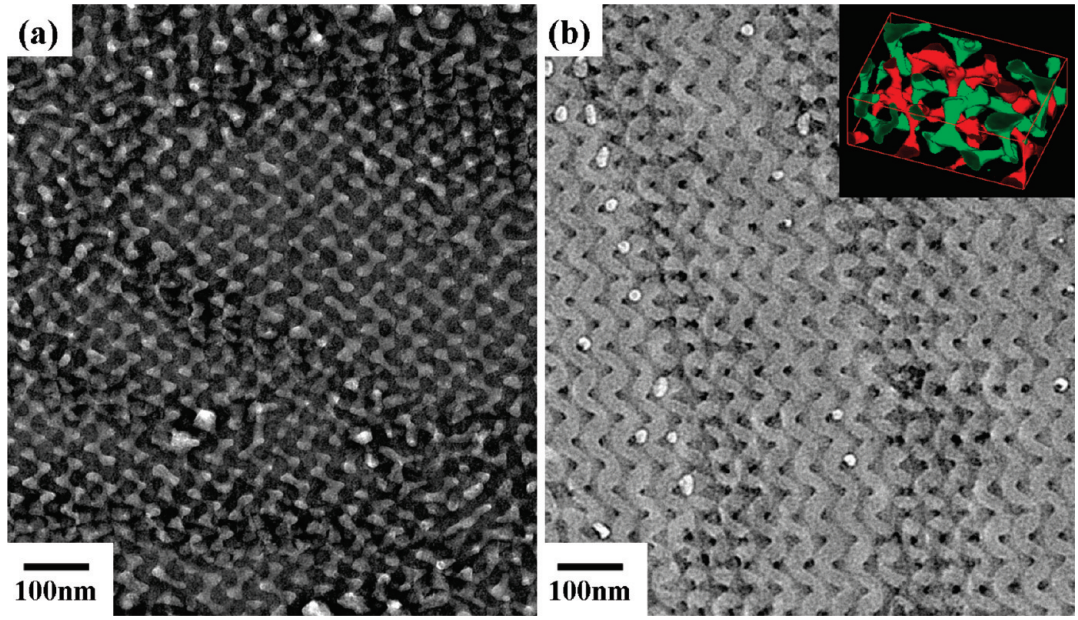

FIGURE 2. TEM micrographs of (a) RuO_4 staining PS-PLLA gyroid nanostructures corresponding to the [100] projection; (b) the [100] projected image of the PS/SiO_2 gyroid nanohybrids without staining. Inset shows the reconstructed 3D image of the SiO_2 gyroid nanostructure (the double gyroid nanostructure) in the nanohybrid.

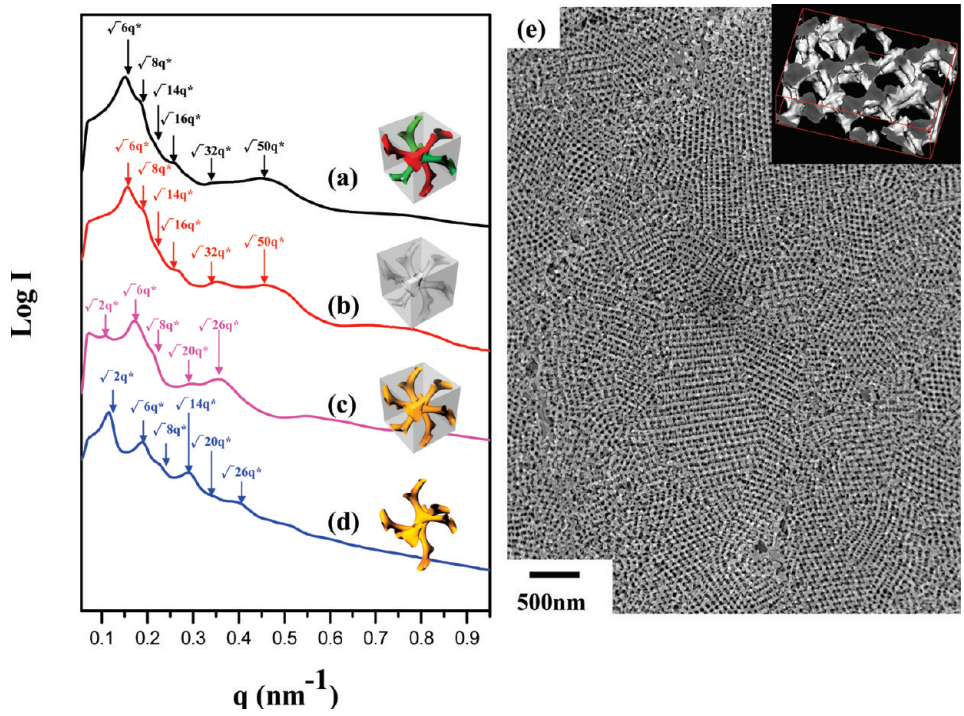

FIGURE 3. One-dimensional SAXS profiles of (a) PS-PLLA BCP after quenching from microphase-separated ordered melt; (b) nanoporous PS template after the removal of the PLLA blocks of PS-PLLA BCP by hydrolysis; (c) PS/SiO_2 gyroid nanohybrids; (d) nanoporous gyroid SiO_2. (e) FESEM micrograph of nanoporous gyroid SiO_2 from PS/SiO_2 gyroid nanohybrids after the UV removal of PS template. Inset shows the reconstructed 3D image of the nanoporous gyroid SiO_2 nanostructure (the pseudosingle gyorid SiO_2 nanostructure).

microsection. The PS microdomains, selectively stained with RuO_4, appear dark, whereas the PLLA microdomains appear bright. The projection image suggests the formation of a gyroid phase. The corresponding one-dimensional small-angle X-ray scattering (SAXS) (Figure 3a) further confirms the observed BCP gyroid nanostructure; scattering peaks are found at the q^* ratios of $\sqrt{6}$:$\sqrt{8}$:$\sqrt{14}$:$\sqrt{16}$:$\sqrt{32}$:$\sqrt{50}$. The characteristic first two reflections for the samples at a spacing ratio of $\sqrt{6}$ and $\sqrt{8}$ are indicative of gyroid morphology, and all other reflections are relatively weak.[42] The

DOI: 10.1021/nl103104w | Nano Lett. 2010, 10, 4994–5000

interdomain spacing of $(211)_{gyroid}$ ($d_{(211)G}$) was determined to be approximately 40.9 nm from the primary reflection. After hydrolysis in a mild aqueous base, the PLLA blocks of the PS-PLLA bulk samples were removed completely. Figure 3b displays the 1D SAXS profile of the PS-PLLA samples following hydrolysis; the diffraction peaks are at the q^* ratios of $\sqrt{6}$:$\sqrt{8}$:$\sqrt{14}$:$\sqrt{16}$:$\sqrt{32}$:$\sqrt{50}$. According to the SAXS results of the PS/air sample, the gyroid morphology was retained upon the removal of the PLLA blocks. Furthermore, nitrogen adsorption experiments were used to measure the porosity of the nanoporous PS template. The porosity of the nanoporous PS template is about 37%, approximately equal to the volume fraction of the PLLA block (39%) of intrinsic PS-PLLA bulk sample. The interfacial area per gram of the nanoporous PS templates can be determined as 97 m^2/g from Brunauer−Emmett−Teller analyzer (BET) analysis. Consequently, bicontinuous nanochannels were fabricated and employed as a nanoporous PS template for the following sol−gel process to synthesize organic/inorganic nanohybrids.

A sol−gel reaction mixture of tetraethoxysilane (TEOS), HCl (0.1M), and methanol was introduced into the PS template with stirring at room temperature for 24 h and then aged at controlled humidity at 50 °C in an oven for 48 h. After aging and then drying under ambient atmosphere, the PS/SiO_2 gyroid hybrid nanostructure was found. Figure 2b presents the [100] projected image of the PS/SiO_2 gyroid nanohybrids without RuO_4 staining. The projected image in Figure 2b is similar to Figure 2a; nevertheless, the contrast is reversed because the PLLA blocks are completely removed after hydrolysis and the formation of the solid SiO_2 is successfully templated by the nanoporous PS matrix via the sol−gel process. The inset of Figure 2b displays the reconstructed 3D image of the SiO_2 gyroid nanostructure in the nanohybrids by reconstruction from a set of 2D images at different tilt angles for projection (see Supporting Information for experimental details). Figure 3c shows 1D SAXS result for the PS/SiO_2 gyroid nanohybrids. On the basis of the characteristic first two reflections for the gyroid nanohybrids at a spacing ratio of $\sqrt{6}$ and $\sqrt{8}$, the interdomain spacing is reduced to approximately 37.8 nm, which compares with the original value of 40.9 nm obtained in the nanoporous PS template; the experimental results indicate that the PS/SiO_2 gyroid nanohybrids shrinks by about 7.5% of their original size after the sol−gel reaction. We suggest that the change in the interdomain spacing results from the swelling of the PS matrix by the solution and the formation of SiO_2 dry gel, leading to a reduction in proportional dimension of the gyroid feature over the aging period. As a result, a well-defined bicontinuous SiO_2 double gyroid network in a PS matrix can be formed by carrying out a low-temperature sol−gel reaction within the gyroid nanochannels through templating (see Supporting Information for experimental details). Also, it is noted that there are variations in the scattering profile; the q^* ratios of $\sqrt{6}$:$\sqrt{8}$:$\sqrt{20}$:$\sqrt{26}$ is different to the intrinsic PS-PLLA and the nanoporous PS. In particular, a new peak labeled with $\sqrt{2}$ can be identified. The variations might be attributed to the deformation of the gyroid nanostructure resulting in the formation of (110) reflection ($\sqrt{2}$ peak),[43,44] as compared to the (211) and (220) reflections for $\sqrt{6}$ and $\sqrt{8}$ diffractions (see below for detailed discussion).

The PS/SiO_2 gyroid nanohybrids were further treated by exposure to UV under atmospheric condition for 24 h with a UV source (wavelength = 254 nm and intensity = 3mW/cm^2) to remove the PS matrix. Fourier transform infrared spectroscopic (FT-IR) can be used to confirm that the PS was completely removed after UV irradiation. Figure 3e shows the texture of the nanoporous gyroid SiO_2 materials. Figure 3d displays the 1D SAXS profile of the nanoporous gyroid SiO_2 materials; the diffraction peaks are at the q^* ratios of $\sqrt{2}$:$\sqrt{6}$:$\sqrt{8}$:$\sqrt{14}$:$\sqrt{20}$:$\sqrt{26}$. In contrast to the scattering results from the PS/SiO_2 gyroid nanohybrids, the $\sqrt{2}$ peak can be clearly identified and there are extra diffractions appearing. As described, the appearance of the $\sqrt{2}$ reflection might be attributed to the deformation of the gyroid nanostructure (i.e., the formation of anisotropic gyroid nanostructure),[43,44] but the expected (110) reflection (i.e., $\sqrt{4}$ peak) is missing. Consequently, in contrast to the typical double gyroid nanostructure from BCPs with a space group of $Ia\bar{3}d$, we speculate that those characteristic reflections at the q^* ratios of $\sqrt{2}$:$\sqrt{6}$:$\sqrt{8}$:$\sqrt{14}$:$\sqrt{20}$:$\sqrt{26}$ result from a pseudosingle gyroid nanostructure with a space group of $I4_132$; a single gyroid nanostructure has been found in lycaenid and papilionid butterflies and corresponding scattering results were well characterized.[45] Namely, the variations in the reflections suggest a phase transformation from double gyroid to pseudosingle gyroid nanostructure during the removal of the PS matrix. The texture of the nanoporous gyroid SiO_2 materials with a pseudosingle gyroid nanostructure can be clearly evidenced by the reconstructed 3D image, as shown in the inset of Figure 3e. The study of the transformation mechanism from double gyroid networks to a pseudosingle gyroid network is still in progress. The porosity of the nanoporous gyroid SiO_2 materials is about 66% from nitrogen adsorption experiments. Surprisingly, the interfacial area per gram of the nanoporous gyroid SiO_2 materials was calculated as 790 m^2/g, which is one order magnitude higher than the ordinary porous materials and an order of magnitude similar with that of common zeolites.

Because of the high porosity of the air voids and low refractive index of amorphous SiO_2 that is synthesized by the sol−gel process, nanoporous gyroid SiO_2 materials can be expected to possess extremely low refractive indices. To measure the refractive indices, testing samples could be obtained by either spin coating or ultramicrotomy from the bulk samples of the gyroid-forming nanostructures with different constituents. To precisely control the sample thickness and also to avoid the thickness and substrate effect on the nanostructure formation of thin films, testing samples for the following experiments were obtained by ultramicro-

DOI: 10.1021/nl103104w | Nano Lett. 2010, 10, 4994--5000

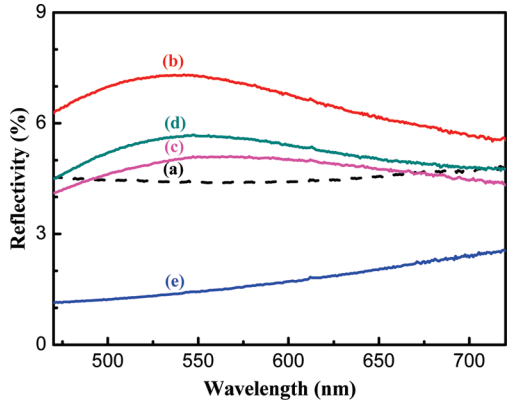

FIGURE 4. Normal-incidence reflectances of (a) quartz and gyroid-forming nanostructures with different constituents: (b) PS-PLLA BCP; (c) nanoporous PS template; (d) PS/SiO_2 gyroid nanohybrids; and (e) nanoporous gyroid SiO_2 on quartz substrate.

tomy from the bulk samples. Consequently, testing samples with different constituents were transferred onto quartz substrates and then measured by alpha-step profilometer to confirm the thickness. Figure 4 shows the reflectances of the gyroid-forming nanostructures with various constituents. The normal-incident reflection spectra were obtained using a homemade optical microscope with a 10× objective lens (Olympus, MPlan, N.A. = 0.25). The effective refractive index (n_{eff}) of the nanostructures can be described by the Fresnel equation in multilayer interference systems. At normal incidence, the amplitude reflection coefficient of the air/nanostructures interface is $r_1 = (1 - n_{eff})/(1 + n_{eff})$, and the amplitude reflection coefficient of the nanostructures/quartz interface is $r_2 = (n_{eff} - n_q)/(n_{eff} + n_q)$, where n_q is the refractive index of quartz. Therefore, the amplitude reflection coefficient of the totally reflected light (r) can be obtained by summing an infinite series of partially reflected waves after multiple reflections within the nanostructured materials. The resulting reflectivity is

$$R = |r|^2 = \left| \frac{r_1 + r_2 e^{i\varphi}}{1 + r_1 r_2 e^{i\varphi}} \right|^2 \quad (1)$$

where φ is the phase difference associated with the optical path within the nanostructured materials and $\varphi = 4\pi n_{eff}\, d/\lambda$ where d is the thickness of ARS and n_{eff} is the effective refractive index of nanostructured materials. Therefore, the n_{eff} can be estimated according to the measured reflectivity. As shown in Figure 4, the black dashed line (Figure 4a) represents the reflectivity of a quartz substrate with a refractive index of approximately 1.5. By contrast, the refractive index of polymers is normally around 1.5−1.6. The refractive index of PS is approximately 1.6. As a result, the PS-PLLA BCP thin-film sample has the highest reflectivity (Figure 4b) due to the high refractive indices of polymers. After hydrolysis, the nanoporous PS template with gyroid-forming nanochannels was obtained so as to reduce the reflectivity (Figure 4c) due to the formation of air voids. For the templated sol−gel process, the formation of SiO_2 is reasonably anticipated to slightly increase the reflectivity of the template, because the refractive index of SiO_2 is certainly higher than that of air ($n \sim 1$). Accordingly, the reflectivity of the PS/SiO_2 gyroid nanohybrids (Figure 4d) is in between that of the PS-PLLA BCP and that of the nanoporous PS template. The porosities of the PS template and the nanoporous gyroid SiO_2 bulk from BET measurements are determined to be 37 and 66%; the higher porosity for the nanoporous gyroid SiO_2 than the constituted volume fraction of the PS block (61%) after the PS part is removed by UV degradation is attributed to the presence of voids in the amorphous SiO_2 matrix after the evaporation of solvent. The amorphous SiO_2 forming after the sol−gel process has a lower refractive index than that of dense and amorphous SiO_2 ($n = 1.45$). Owing to the high porosity of the air voids and low refractive index of amorphous SiO_2 from the sol−gel process, the nanoporous gyroid SiO_2 thus exhibits a significant antireflection property as expected (Figure 4e). Most interestingly, the low reflectivity of the nanoporous gyroid SiO_2 is evident over the whole spectral range of visible light and it is nearly independent of wavelength. We speculate that the fluctuation of reflectance curve might be attributed to the scattering from the structures of materials such as grain boundaries.

The excellent antireflection property of the nanoporous gyroid SiO_2 is attributed to its high porosity and well-defined periodic nanostructures. Namely, the formation of inorganic nanoporous materials with low refractive index can be achieved. Because the reflectivity of the nanoporous gyroid SiO_2 with a thickness of 200 nm is ~2.4% at $\lambda = 600$ nm, the n_{eff} can be estimated to be 1.1 for $\lambda = 600$ nm (See Figure S3 of Supporting Information). Furthermore, the relationship between the sample thickness and reflectivity can also be measured by Fresnel equation in multilayer interference systems as shown in Supporting Information Figure S4. The black line means the refractive index equal to 1.1 at $\lambda = 600$ nm from theoretical calculation. The reflectivities corresponded to samples with different thicknesses controlled by ultramicrotomy nearly locate on the black line ($n = 1.1$), indicating the n_{eff} of the nanoporous gyroid SiO_2 is reliable.

Accordingly, the refractive index of nanoporous gyroid SiO_2 can also be determined by Bruggemann effective medium approximation, given below.[46,47]

$$f\frac{n_1^2 - n_{eff}^2}{n_1^2 + 2n_{eff}^2} + (1 - f)\frac{n_2^2 - n_{eff}^2}{n_2^2 + 2n_{eff}^2} = 0 \quad (2)$$

where n_1 and n_2 are the refractive indices of the air and SiO_2, respectively, and f is the volume fraction of air voids in the nanoporous gyroid SiO_2. With $f = 0.66$, $n_1 = 1.0$ and $n_2 =$

DOI: 10.1021/nl103104w | Nano Lett. 2010, 10, 4994–5000

1.30 (the refractive index of amorphous SiO_2 synthesized via the sol−gel process, as measured in this study), the refractive index of nanoporous gyroid SiO_2 is determined to be 1.1. This value is also in good agreement with the reflectivity measurements, indicating that the Bruggemann effective medium approximation works well for this hybrid material system.

Note that for practical applications it is much appealing to have large-size thin-film samples with gyroid-forming nanostructures; we simply used spin-coating process to achieve the thickness control of uniform thin-film samples from BCP self-assembly in this study. Although decades of researches have provided a foundation for understanding BCP self-assembly in thin films,[5,48] the control of thin-film morphologies still remains a challenge. In principle, thin-film BCP self-assembly is primarily dependent upon the process for thin-film formation that is usually a kinetically controlled origin regardless of substrate effect.[49] Consistently, for the BCP system (PS-PLLA) we examined here, well-oriented, perpendicular PLLA cylinders of PS-PLLA thin films could be efficiently achieved by spin coating using appropriate solvents for various substrates.[50] The equilibrium origins take over while the BCP thin films are thermally treated or annealed by the vapor of good nonpreferential solvent (i.e., solvent annealing). Consequently, the morphological evolution would be strongly dependent upon the roles of air surface and interfacial effect. Moreover, the effect of thin-film thickness (i.e., the confinement effect) might be effective once the film thickness reaches a minimum at which an integer multiple of a natural layer thickness is energetically favored.[51] Accordingly, the control of thin-film morphologies for BCP self-assembly would be dependent upon the surface energy of constituted components and their interactions with substrate as well as the thickness of thin-film samples. Consequently the phase behavior of BCP thin film, such as the order−disorder and order−order transition boundaries, might be varied with the thickness and also affected by the effects of air surface and substrate.

In this study, to achieve a well-defined gyroid nanostructure with controlled thickness of around 150 nm (see Figure S5 in Supporting Information for the details of thickness control) satisfying the dimension requirement as antireflection structure for visible light, spin-coating process for thin-film formation was carried out first so as to create thin films with uniform thickness. Subsequently, solvent-annealing process was conducted to acquire the equilibrium morphology as gyroid nanostructure with large-scale orientation. To alleviate the effect of substrate, chemically modified substrate was prepared by using polystyrene with hydroxyl chain end. A substrate with a neutral or nonpreferential wetting of the substrate for PS-PLLA could be prepared from this modification. As shown in Figure S6 in Supporting Information, the thin-film morphologies are different to the morphology of bulk sample when the thickness of the PS-PLLA thin films is approximately smaller than 4 times of the *d*-spacing of the $(211)_G$ planes. As a result, the equilibrium morphology as gyroid nanostructure can be obtained for samples with thickness larger than 130 nm (see Figure S7 in Supporting Information). Although it is possible to cause surface roughing due to the solvent-annealing treatment, the variation in thickness can be reasonably controlled by dedicated solvent removal for thick enough samples as the case examined here. Systematic study is still in progress to examine the morphological variation and corresponding evolution of thin-film morphologies in self-assembled PS-PLLA BCPs with asymmetry compositions.

Similar procedure for templated sol−gel process by using hydrolyzed PS-PLLA as templates can be carried out for the formation of PS/SiO_2 nanohybrids (see Supporting Information for details). Consequently, similar testing samples as described could be prepared. For practical applications, different coating processes, such as slot coating and gravure coating, should be available to provide cost-effective approaches for the formation of large-area coatings. In fact, a tentative test has been done by using blade-coating method for the purpose. It is noted that the formation of the thin-film sample with gyroid nanostructure is thermodynamically driven process via solvent-annealing treatment in this work. As a result, similar results for the control of morphological evolution from BCP self-assembly and templating can be achieved. The integration of thin-film technologies and ARS formation described here for practical applications in optoelectronics such as backlight module in display applications is still in progress.

Supporting Information Figure S8 presents the normal-incident transmission spectra of the gyroid-forming nanostructures with different constituents on quartz substrates. The black dashed line (Supporting Information Figure S8a) represents the transmissivity of a quartz substrate. Apart from the lowest reflectivity among the samples examined, the nanoporous gyroid SiO_2 sample possesses the highest transmission with respect to visible light (400−800 nm), as shown in Supporting Information Figure S8b. Notably, the nanoporous PS template (Supporting Information Figure S8e) suffers from low transmission. We speculate that the cause for the low transmission is attributed to the scattering of visible light in well-defined two-phase materials with significant difference between the refractive indices of the constituents besides the absorbance of PS. Accordingly, the transmissions of the PS/SiO_2 gyroid nanohybrids (Supporting InformationFigure S8c) and the PS-PLLA BCP (Supporting InformationFigure S8d) are higher than that of the nanoporous PS template due to the alleviation of scattering problem. As a result, the formation of inorganic gyroid with low refractive index ($n = 1.1$) can be successfully achieved by BCP templates.

Conclusions. Nanoporous polymers with gyroid nanochannels can be fabricated from the self-assembly of degradable block copolymer, polystyrene-*b*-poly(L-lactide) (PS-PLLA), followed by the hydrolysis of PLLA blocks. Well-

DOI: 10.1021/nl103104w | *Nano Lett.* **2010,** *10,* 4994–5000

defined nanohybrids with SiO_2 gyroid nanostructures in a PS matrix can be obtained using nanoporous PS as a template for the sol−gel reaction. After the removal of the PS matrix, the nanohybrids can be transferred to a highly porous inorganic gyroid network. Because of the high porosity of the air voids and extremely low refractive index (as low as 1.1) of nanoporous gyroid SiO_2, it provides the appealing applications as ARS materials with high transmission and low reflection properties as well as superior environmental resistance.

Acknowledgment. The authors would like to thank the National Science Council of the Republic of China, Taiwan, for financially supporting this research under Contract No. NSC 99-2120-M-007-003. Also, this research was supported by United States National Science Foundation (NSF) (Grant DMR 0804449) for partial financial support. Ms. I.-H. Wu of the Department of Applied Chemistry at NCTU is appreciated for her assistance in the FESEM experiments, as well the National Synchrotron Radiation Research Center (NSRRC), Taiwan for its assistance in the Synchrotron SAXS experiments.

Supporting Information Available. Experimental information, additional figures, and movie. This material is available free of charge via the Internet at http://pubs.acs.org.

REFERENCES AND NOTES

(1) Fleisher, R. L.; Price, P. B.; Walker, R. M. *Nuclear Tracks in Solids*; University of California Press: Berkeley, CA., 1975,
(2) Furneaux, R. C.; Rigby, W. R.; Davidson, A. P. *Nature* **1989**, *337*, 147–149.
(3) Bates, F. S.; Fredrickson, G. H. *Annu. Rev. Phys. Chem.* **1990**, *41*, 525–557.
(4) Bates, F. S.; Fredrickson, G. H. *Phys Today* **1999**, *52*, 32–38.
(5) Park, M.; Harrison, C.; Chaikin, P. M.; Register, R. A.; Adamson, D. H. *Science* **1997**, *276*, 1401–1404.
(6) Thurn-Albrecht, T.; Steiner, R.; DeRouchey, J.; Stafford, C. M.; Huang, E.; Bal, M.; Tuominen, M.; Hawker, C. J.; Russell, T. P. *Adv. Mater.* **2000**, *12*, 787–791.
(7) Cheng, J. Y.; Ross, C. A.; Thomas, E. L.; Smith, H. I.; Vancso, G. J. *Appl. Phys. Lett.* **2002**, *81*, 3657–3659.
(8) Zalusky, A. S.; Olayo-Valles, R.; Taylor, C. J.; Hillmyer, M. A. *J. Am. Chem. Soc.* **2001**, *123*, 1519–1520.
(9) Hashimoto, T.; Tsutsumi, K.; Funaki, Y. *Langmuir* **1997**, *13*, 6869–6872.
(10) Chan, V.Z.-H.; Hoffman, J.; Lee, V. Y.; Latrou, H.; Avgeropoulos, A.; Hadjichristidis, N.; Miller, R. D.; Thomas, E. L. *Science* **1999**, *286*, 1716–1719.
(11) (a) Tseng, W. H.; Chen, C. K.; Chiang, Y. W.; Ho, R. M.; Akasaka, S.; Hasegawa, H. *J. Am. Chem. Soc.* **2009**, *131*, 1356–1357. (b) Ho, R.-M.; Chiang, Y.-W.; Chen, C.-K.; Wang, H.-W.; Hasegawa, H.; Akasaka, S.; Thomas, E. L.; Burger, C.; Hsiao, B. S. *J. Am. Chem. Soc.* **2009**, *131*, 18533–18542.
(12) Hajduk, D. A.; Harper, P. E.; Gruner, S. M.; Honeker, C. C.; Kim, G.; Thomas, E. L.; Fetters, L. J. *Macromolecules* **1994**, *27*, 4063–4075.
(13) Schulz, M. F.; Bates, F. S.; Almdal, K.; Mortensen, K. *Phys. Rev. Lett.* **1994**, *73*, 86–89.
(14) Matsen, M. W.; Schick, M. *Phys. Rev. Lett.* **1994**, *72*, 2660–2663.
(15) Martin-Moreno, L.; Garcia-Vidal, F. J.; Somoza, A. M. *Phys. Rev. Lett.* **1999**, *83*, 73–75.
(16) Urbas, A. M.; Maldovan, M.; DeRege, P.; Thomas, E. L. *Adv. Mater.* **2002**, *14*, 1850–1853.
(17) Finnefrock, A. C.; Ulrich, R.; Toombes, G. E. S.; Gruner, S. M.; Wiesner, U. *J. Am. Chem. Soc.* **2003**, *125*, 13084–13093.
(18) Jain, A.; Toombes, G. E. S.; Hall, L. M.; Mahajan, S.; Garcia, C. B. W.; Probst, W.; Gruner, S. M.; Wiesner, U. *Angew. Chem., Int. Ed.* **2005**, *44*, 1226–1229.
(19) Adachi, M.; Okumura, A.; Sivaniah, E.; Hashimoto, T. *Macromolecules* **2006**, *39*, 7352–7357.
(20) Urade, V. N.; Wei, T. C.; Tate, M. P.; Kowalski, J. D.; Hillhouse, H. W. *Chem. Mater.* **2007**, *19*, 768–777.
(21) Finnemore, A. S.; Scherer, M. R. J.; Langford, R.; Mahajan, S.; Ludwigs, S.; Meldrum, F. C.; Steiner, U. *Adv. Mater.* **2009**, *21*, 3928–3932.
(22) Ndoni, S.; Li, L.; Schulte, L.; Szewezykowski, P. P.; Hansen, T. W.; Guo, F. X.; Berg, R. H.; Vigild, M. E. *Macromolecules* **2009**, *42*, 3877–3880.
(23) Crossland, E. J. W.; Kamperman, M.; Nedelcu, M.; Ducati, C.; Wiesner, U.; Smilgies, D. M.; Toombes, G. E. S.; Hillmyer, M. A.; Ludwigs, S.; Steiner, U.; Snaith, H. J. *Nano Lett.* **2009**, *9*, 2807–2812.
(24) Lee, Y. J.; Ruby, D. S.; Peters, D. W.; Mckenzie, B. B.; Hsu, J. W. P. *Nano Lett.* **2008**, *8*, 1501–1505.
(25) Xi, J. Q.; Ojha, M.; Plawsky, J. L.; Gill, W. N.; Kim, J. K.; Schubert, E. F. *Appl. Phys. Lett.* **2005**, *87*, 031111−1031111−3.
(26) Southwell, W. H. *Opt. Lett.* **1983**, *8*, 584–586.
(27) Lohmüller, T.; Helgert, M.; Sundermann, M.; Brunner, R.; Spatz, J. P. *Nano Lett.* **2008**, *8*, 1429–1433.
(28) An, S. J.; Chae, J. H.; Yi, G. C.; Park, G. H. *Appl. Phys. Lett.* **2008**, *92*, 121108-1–121108-3.
(29) Thomas, I. M. *Appl. Opt.* **1992**, *31*, 6145–6149.
(30) Xi, J. Q.; Ojha, M.; Cho, W.; Plawsky, J. L.; Gill, W. N.; Gessmann, T.; Schubert, E. F. *Opt. Lett.* **2005**, *30*, 1518–1520.
(31) Walheim, S.; Schaeffer, E.; Mlynek, J.; Steiner, U. *Science* **1999**, *283*, 520–522.
(32) Joo, W.; Park, M. S.; Kim, J. K. *Langmuir* **2006**, *22*, 7960–7963.
(33) Cho, J. H.; Hong, J. K.; Char, K.; Caruso, F. *J. Am. Chem. Soc.* **2006**, *128*, 9935–9942.
(34) Kanamori, Y.; Sasaki, M.; Hane, K. *Opt. Lett.* **1999**, *24*, 1422–1424.
(35) Rüetschi, M.; Grütter, P.; Fünfschilling, J.; Güntherodt, H. J. *Science* **1994**, *265*, 512–514.
(36) Ibn-Elhaj, M.; Schadt, M. *Nature* **2001**, *410*, 796–799.
(37) Wilson, S. J.; Hutley, M. C. *Opt. Acta* **1982**, *7*, 993–1009.
(38) Clapham, P. B.; Hutley, M. C. *Nature* **1973**, *244*, 281–282.
(39) Motamedi, M. E.; Southwell, W. H.; Gunning, W. J. *Appl. Opt.* **1992**, *31*, 4371–4376.
(40) Lalanne, P.; Morris, G. M. *Nanotechnology* **1997**, *8*, 53–56.
(41) Hench, L. L.; West, J. K. *Chem. Rev.* **1990**, *90*, 33–72.
(42) Hajduk, D. A.; Harper, P. E.; Gruner, S. M.; Honeker, C. C.; Kim, G.; Thomas, E. L.; Fetter, L. J. *Macromolecules* **1994**, *27*, 4063–4075.
(43) Dair, B. J.; Honeker, C. C.; Alward, D. B.; Avgeropoulos, A.; Hadjichristidis, N.; Fetters, L. J.; Capel, M.; Thomas, E. L. *Macromolecules* **1999**, *32*, 8145–8152.
(44) Sakurai, S.; Isobe, D.; Okamoto, S.; Yao, T.; Nomura1, S. *Phys. Rev. E* **2001**, *63*, 061803−1061803−5.
(45) Saranathan, V.; Osuji, C. O.; Mochrie, S. G. J.; Noh, H.; Narayanan, S.; Sandy, A.; Dufresne, E. R.; Prum, R. O. *Proc. Natl. Acad. Sci. U.S.A.* **2010**, *107*, 11676.
(46) Aspnes, D. E. *Thin Solid Films* **1982**, *89*, 249–262.
(47) Chen, H. Y.; Lin, H. W.; Wu, C. Y.; Chen, W. C.; Chen, J. S.; Gwo, S. *Opt. Express* **2008**, *16*, 8106–8116.
(48) (a) Lammertink, R. G. H.; Hempenius, M. A.; van den Enk, J. E.; Chan, V. Z.-H.; Thomas, E. L.; Vancso, G. J. *Adv. Mater.* **2000**, *12*, 98–103. (b) Lin, Z.; Kim, D. H.; Wu, X.; Boosahda, L.; Stone, D.; LaRose, L.; Russell, T. P. *Adv. Mater.* **2002**, *14*, 1373–1376. (c) Kim, S. H.; Misner, M. J.; Xu, T.; Kimura, M.; Russell, T. P. *Adv. Mater.* **2004**, *16*, 226–231. (d) Qiao, Y.; Wang, D.; Buriak, J. M. *Nano Lett.* **2007**, *7*, 464–469. (e) Albert, J. N. L.; Epps, T. H., III. *Mater. Today* **2010**, *13*, 24–33.
(49) Kim, G.; Libera, M. *Macromolecules* **1998**, *31*, 2569.
(50) (a) Tseng, Y. T.; Tseng, W. H.; Lin, C. H.; Ho, R. M. *Adv. Mater.* **2007**, *19*, 3584–3588. (b) Ho, R. M.; Tseng, W. H.; Fan, H. W.; Chiang, Y. W.; Lin, C. C.; Ko, B. T.; Huang, B. H. *Polymer* **2005**, *46*, 9362–9377.
(51) Knoll, A.; Horvat, A.; Lyakhova, K. S.; Krausch, G.; Sevink, G. J. A.; Zvelindovsky, A. V.; Magerle, R. *Phys. Rev. Lett.* **2002**, *89*, 035501-1–035501-4.

DOI: 10.1021/nl103104w | *Nano Lett.* **2010,** *10,* 4994–5000